⌘ Author's Choice

Alkylation Damage by Lipid Electrophiles Targets Functional Protein Systems*[S]

Simona G. Codreanu‡, Jody C. Ullery‡, Jing Zhu§, Keri A. Tallman¶, William N. Beavers¶, Ned A. Porter¶, Lawrence J. Marnett‡¶, Bing Zhang§, and Daniel C. Liebler‡§‖

Protein alkylation by reactive electrophiles contributes to chemical toxicities and oxidative stress, but the functional impact of alkylation damage across proteomes is poorly understood. We used Click chemistry and shotgun proteomics to profile the accumulation of proteome damage in human cells treated with lipid electrophile probes. Protein target profiles revealed three damage susceptibility classes, as well as proteins that were highly resistant to alkylation. Damage occurred selectively across functional protein interaction networks, with the most highly alkylation-susceptible proteins mapping to networks involved in cytoskeletal regulation. Proteins with lower damage susceptibility mapped to networks involved in protein synthesis and turnover and were alkylated only at electrophile concentrations that caused significant toxicity. Hierarchical susceptibility of proteome systems to alkylation may allow cells to survive sublethal damage while protecting critical cell functions. ***Molecular & Cellular Proteomics 13: 10.1074/mcp.M113.032953, 849–859, 2014.***

Covalent protein alkylation by reactive electrophiles was identified as a key triggering event in chemical toxicity over 40 years ago (1, 2). These reactions remain a major cause of drug toxicity and represent a longstanding problem in drug safety (3). Oxidative stress also generates reactive lipid electrophiles, which covalently modify proteins and trigger stress signaling and cell death associated with inflammation and degenerative diseases (4–6). Despite the broad importance of this problem, the mechanisms by which protein alkylation drives toxicity remain largely unexplained. Interestingly, some drug molecules produce significant protein covalent binding without causing toxicity (7, 8), which suggests that a only critical subset of protein alkylation events contribute to injury. Thus, the major challenge in this field is to distinguish toxic from nontoxic protein alkylation damage.

We and others have explored this problem by combining electrophile probes and MS-based proteomics to perform systematic, global inventories of protein alkylation damage. These studies revealed electrophile-specific patterns of protein alkylation, yet also indicated that many proteins are targets of multiple electrophiles (9) (10–13). Inference of possible toxicity mechanisms from such inventories is complicated by the diversity of biological processes represented by electrophile protein targets. However, we have recently reported that combined analysis of protein target inventories with transcriptome expression profiles enables inference of candidate networks associated with activation of stress responses (14). Thus, functional readouts of damage effects could guide interpretation of protein adduct profiles.

An important limitation of most previous protein adduct profiling studies is that they were done in subcellular fractions or cell lysates, which lack intact detoxification mechanisms for electrophiles, particularly glutathione (GSH)[1]-dependent conjugation. The onset of toxicity in both cell and animal models often coincides with GSH depletion and an increase in covalent protein binding (15). Analysis of protein adduct profile changes accompanying GSH depletion thus may provide another means to interpret the effects of protein damage.

To address these questions, we performed a series of quantitative adduct profiling experiments with alkynyl analogs of the prototypical lipid electrophiles 4-hydroxy-2-nonenal (HNE) and 4-oxo-2-nonenal (ONE). The alkynyl analogs (aHNE and aONE, supplemental Fig. S1*A* and S1*B*) form adducts that can be biotinylated during sample workup by Huisgen 1,3-dipolar cycloaddition (Click chemistry) for efficient, high affinity capture for subsequent proteomic analysis (16). Use of a photocleavable azidobiotin reagent enables photorelease from streptavidin under mild conditions, thus reducing background contamination with non-adducted proteins (17).

From the ‡Department of Biochemistry, Vanderbilt University School of Medicine, Nashville, Tennessee 37232; §Department of Biomedical Informatics, Vanderbilt University School of Medicine, Nashville, Tennessee 37232; ¶Department of Chemistry, Vanderbilt University, Nashville, Tennessee 37235

⌘ *Author's Choice*—Final version full access.

Received July 30, 2013, and in revised form, January 6, 2014

Published, MCP Papers in Press, January 15, 2014, DOI 10.1074/mcp.M113.032953

Author contributions: N.A.P., L.J.M., B.Z., and D.C.L. designed research; S.G.C., J.C.U., K.A.T., and W.N.B. performed research; N.A.P. and B.Z. contributed new reagents or analytic tools; S.G.C., J.C.U., J.Z., K.A.T., W.N.B., B.Z., and D.C.L. analyzed data; S.G.C., K.A.T., W.N.B., B.Z., and D.C.L. wrote the paper.

[1] The abbreviations used are: GSH, glutathione; ONE, 4-oxo-2-nonenal; HNE, 4-hydroxy-2-nonenal; FDR, false discovery rate.

MATERIALS AND METHODS

Materials—McCoy's 5A Medium, RPMI 1640 Medium, phosphate-buffered saline 1X (PBS), NuPAGE® 10% SDS-gels, MES SDS running buffer, Simply Blue Safe stain were purchased from Invitrogen (Carlsbad, CA). Streptavidin Sepharose™ High Performance beads were obtained from GE Healthcare (Uppsala, Sweden). Trypsin Gold™ was purchased from Promega (Madison, WI). FBS was obtained from Atlas Biologicals (Fort Collins, CO). aHNE was synthesized as previously described (16) and reconstituted in ethanol as a 200 mM stock solution stored at −80 °C. All other chemicals were obtained from Sigma-Aldrich Chemical Co. (St. Louis, MO) and were used without further purification.

Synthesis of aONE—Dess-Martin periodinane (2.0 g, 4.6 mmol) was added to a solution of aHNE (0.57 g, 3.8 mmol) in CH_2Cl_2 (18 ml). After 1 h, the reaction mixture was diluted with EtOAc and washed with H_2O, brine, and dried over $MgSO_4$. The product was purified by column chromatography (20% EtOAc/hexanes) and isolated as a yellow oil (0.46 g, 83%). ^{1}H NMR ($CDCl_3$) δ 9.66 (d, 1H, J = 7.1 Hz), 6.81 (d, 1H, J = 16.3 Hz), 6.67 (dd, 1H, J = 7.1, 16.3 Hz), 2.76 (t, 2H, J = 7.1 Hz), 2.15 (dt, 2H, J = 2.6, 6.8 Hz), 1.91 (t, 1H, J = 2.6 Hz), 1.74 (pentet, 2H, J = 6.9 Hz); ^{13}C NMR ($CDCl_3$) δ 199.3, 193.5, 144.7, 137.3, 83.1, 69.6, 39.4, 21.9, 17.5; HRMS (ESI) calculated (M+H) 151.0754, observed 151.0766.

Cell Culture and In Vivo Chemical Treatment—Human colorectal carcinoma (RKO) cells (ATCC no: CRL-2577) were purchased from ATCC (Manassas, Virginia) and were maintained in McCoy's 5A Medium supplemented with 10% fetal bovine serum. Cells were grown in humidified cell culture incubators under 5% CO_2 and 95% air.

Human monocytic leukemia (THP-1) cells (ATCC no: TIB-202) were purchased from ATCC (Manassas, Virginia) and were maintained in RPMI 1640 Medium supplemented with 10% fetal bovine serum, 1 mM L-glutamine, 1x antibiotic/antimycotic (Invitrogen), and 1x MEM vitamins (Mediatech). Cells from suspension cultures were plated at ~25 × 10^6 cells/plate in 150 mm plates and treated with 100 nM phorbol myristate acetate (PMA) for 72h to induce differentiation into human macrophage-like cells.

Treatments with aONE and aHNE were carried out at 37 °C in an atmosphere of 95% air, 5% CO_2 with either varying concentrations of chemicals (0, 5, 10, 20, 50 μM) for 1h or with 50 μM aHNE or aONE for 30 min to 8h to optimize the amount of time for adduct generation. Cells treated with ethanol vehicle (≤0.1% of the total medium volume) were used as controls. During treatments, cultures were maintained in the culture medium described above without serum. Following treatment, cells were harvested, centrifuged at 100 × *g* for 5 min, washed once with 1X PBS, pH 7.4, and stored at −80 °C until use. Samples from vehicle control-treated (EtOH) cells were processed in the same manner. Three independent biological replicate experiments were performed for each control, aHNE or aONE treatment concentration, and each biological replicate experiment was analyzed once by LC-MS-MS.

Click Labeling of Adducted Proteins—To biotinylate aHNE- and aONE-adducted proteins, treated cell pellets were resuspended in cold NETN lysis buffer containing 50 mM HEPES buffer supplemented with 150 mM NaCl, 1% Igepal, and in house made protease inhibitor mixture (0.5 mM AEBSF, 1 mM leupeptin, 10 mM aprotinin, 10 μM pepstatinA, 5 μM bestatin, 1.5 μM E-64) and phosphatase inhibitor mixture (1.0 mM sodium fluoride, 1.0 mM sodium molybdate, 1.0 mM sodium orthovanadate, 10.0 mM β-glycerophosphate) and incubated on ice for 30 min. The lysates were cleared by centrifugation at 10,000 × *g* for 10 min to remove cellular debris and the total protein concentration of the supernatant was determined using the BCA protein assay (Pierce), according to the manufacturer's instructions.

For Click chemistry, 6 mg of each protein lysate (at a concentration of 2 mg/ml in NETN lysis buffer) was reduced with $NaBH_4$ (2 mM) for 1h and the reaction was quenched with acetone. Following reduction, photocleavable N_3-biotin linker (0.2 mM), tris-(2-carboxyethyl) phosphine (TCEP, 1 mM), triazole ligand tris[(1-benzyl-1*H*-1,2,3-triazol-4-yl)methyl]amine (TBTA, 0.1 mM), and Cu_2SO_4 (1 mM) were added, and reaction mixture rotated in the dark for 2 h at room temperature. Proteins were precipitated on ice for 30 min with cold methanol to remove excess reagents (Cu_2SO_4, triazole ligand) from the reaction mixture. Protein pellets were resuspended three times in 1 ml cold methanol with sonication. The mixture was centrifuged at 5000 × *g* for 5 min to remove the supernatant containing excess reagents, then resuspended in 1 ml of 0.5% SDS with sonication (10 pulses, 20% duty cycle) and heated for 5 min at 95 °C to solubilize the proteins. A clear protein solution was obtained, which was further applied to the streptavidin beads.

Streptavidin Capture and Photorelease of Adducted Proteins—Capture and photorelease of Click-labeled aHNE and aONE adducts was done by a modification of our previously published method (17). Biotinylated proteins were resuspended in 0.5% SDS and further diluted to 0.05% SDS with 1X PBS (pH 7.4) and incubated with streptavidin-agarose beads (~ 2 mg protein per 1 ml bead slurry previously equilibrated with PBS) overnight at 4 °C in the dark. All subsequent steps until elution were carried out on ice. After incubation with biotinylated protein, streptavidin-agarose beads were centrifuged at 5000 × *g* for 2 min and the supernatant (flow-through fraction) was discarded. Beads containing the biotinylated proteins were washed (1 ml per wash) in the following sequence: twice with 1% SDS, twice with 4 M urea, twice with 1 M NaCl, twice with phosphate-buffered saline, and twice with H_2O. After each wash, beads were resuspended in the wash solution and then centrifuged at 5000 × *g* for 2 min and the supernatant was discarded. To elute the biotinylated proteins, the streptavidin beads were resuspended in 1 ml of PBS and exposed to UV-light (365 nm) for 90 min at room temperature with stirring. The supernatant was collected and the beads were washed twice with 1X PBS. Proteins were concentrated to a total volume of 100 μl in PBS with 10K molecular weight cutoff Nanosep centrifugal devices that contain an Omega membrane for low protein binding (VWR, San Dimas, CA).

In-gel Digestion of Adducted Proteins—Adducted proteins purified by Click chemistry (as described above) were resolved by 10% SDS-PAGE using NuPAGE® Bis-Tris gels and stained with Simply Blue Safe stain. Bands corresponding to different molecular weights (10 gel fractions for each individual chemical treatment) were excised from the gel and digested in-gel as previously described (13, 18) with the following modifications. After NuPAGE® gel cubes were evaporated to dryness *in vacuo*, they were rehydrated with trypsin (1:20 approximate trypsin/protein mass ratio) in 25 mM ammonium bicarbonate for 15 min at room temperature and then digested by incubation for 22 h at 37 °C. Tryptic peptides were extracted with two rounds of 60% acetonitrile and 0.1% trifluoroacetic acid and the extracts then were evaporated to dryness and reconstituted in 0.1% formic acid.

LC-MS/MS Analysis—Peptide mixtures were subjected to LC-MS/MS analysis on a Thermo LTQ ion trap mass spectrometer (ThermoFisher, San Jose, CA) equipped with an Eksigent Nano-LC 1D plus liquid chromatograph and autosampler (Dublin, CA) and Thermo Nanospray source and Xcalibur 1.4 instrument control. Liquid chromatography was carried out at ambient temperature at a flow rate of 0.6 μl/min using a gradient mixture of 0.1% (v/v) formic acid in water (solvent A) and 0.1% (v/v) formic acid in acetonitrile (solvent B). Centroid MS/MS scans were acquired using an isolation width of 2 *m/z*, an activation time of 30 ms, an activation Q of 0.250 and 30% normalized collision energy, using 1 microscan with a max ion time of 100 ms for each MS/MS scan.

The mass spectrometer was tuned before analysis using the synthetic peptide TpepK (AVAGKAGAR). Some parameters may vary slightly from experiment to experiment, but typically the tune parameters were as follows: spray voltage of 2 KV, a capillary temperature of 150 °C, a capillary voltage of 50 V and tube lens of 120 V. Peptides were resolved on 100 μm × 11 cm fused-silica capillary column (Polymicro Technologies, LLC Phoenix, AZ) packed with 5 μm, 300Å Jupiter C18 (Phenomenex, Torrance, CA). Peptides eluting from the capillary tip were introduced into the LTQ source with a capillary voltage of ~2 kV. The heated capillary was operated at 150 °C and 40 V. MS/MS spectra were acquired in the data-dependent scanning mode, consisting of a full scan obtained for eluting peptides in the range of 400–2000 *m/z*, followed by four data-dependent MS/MS scans, and recorded using dynamic exclusion of previously analyzed precursors for 30 s with a repeat duration of 2 min.

Database Searching—The "ScanSifter" algorithm (19) read MS/MS spectra stored as centroid peak lists from Thermo RAW files and transcoded them to mzData v1.05 files. Spectra that contain fewer than six peaks were not transcoded to mzData files and only MS/MS scans are written to the mzData files; MS scans are excluded. If 90% of the intensity of a tandem mass spectrum appears at a lower *m/z* than the precursor ion, a single precursor charge is assumed; otherwise, the spectrum is processed under both double and triple precursor charge assumptions.

Tandem mass spectra were assigned to peptides from the IPI Human database version 3.56 (May 05, 2009; 153,182 proteins) by the MyriMatch algorithm (20). To estimate false discovery rates, each sequence of the database was reversed and concatenated to the database. Candidate peptides were required to feature trypsin cleavages or protein termini at both ends, though any number of missed cleavages is permitted. All cysteines were expected to undergo carboxamidomethylation and were assigned a mass of 160 kDa. All methionines were allowed to be oxidized. Precursor ions were required to fall within 1.25 *m/z* of the position expected from their average masses, and fragment ions were required to fall within 0.5 *m/z* of their monoisotopic positions. The database searches produced raw identifications in pepXML format.

Peptide identification, filtering, and protein assembly were done with the IDPicker 2.6.271 algorithm (21, 22) where filtering takes place in multiple stages. First, IDPicker filtered raw peptide identification to a target false discovery rate (FDR) of 5%. The peptide filtering employed reversed-sequence database-match information to determine thresholds that yield an estimated 5% FDR for the identifications of each charge state by the formula (23) FDR = $(2R)/(R + F)$, where R is the number of passing reversed-peptide identifications and F is the number of passing forward (normal orientation)-peptide identifications. The second round of filtering removed proteins supported by less than two distinct peptide identifications in the analyses. Indistinguishable proteins were recognized and grouped. Parsimony rules were applied to generate a minimal list of proteins that explain all of the peptides that pass the entry criteria.

Reference Proteome—For the reference proteome databases, cellular lysates for both RKO and THP1 untreated cells were resolved by 10% SDS-PAGE using NuPAGE® Bis-Tris gels, stained with Simply Blue Safe stain, in-gel digested and analyzed by LC-MS-MS as described above. Database searching, peptide identification filtering and protein assembly were done as described above for adducted proteins. One culture of each cell line was analyzed in three technical replicates.

Assessment of Protein Expression Changes Induced by Electrophile Treatment—To determine whether HNE induces protein expression changes under the electrophile exposure conditions, we treated human RKO cells with 0 (vehicle control) or 45 μM HNE for 6h at 37 °C in an atmosphere of 95% air, 5% CO_2. Three independent biological replicate experiments were performed for each treatment concentration and each biological replicate experiment was analyzed once by LC-MS/MS. Cellular lysates for RKO treated cells unenriched this time were resolved by 10% SDS-PAGE using NuPAGE® Bis-Tris gels and stained with Simply Blue Safe stain. Gel lanes were cut into fractions, subjected to in-gel digestion and were analyzed by LC-MS/MS as described above. Database searching, peptide identification filtering and protein assembly were performed as described above for adducted proteins.

Data Analysis and Visualization—To identify proteins differentially expressed in the reference proteomes of the two cell lines or to identify proteins with significantly increased spectral counts in an electrophile-treated sample compared with corresponding untreated sample, the corresponding proteome datasets were analyzed using the Poisson test as previously described (24, 25). To make the spectral counts comparable across different experiments, the spectral counts for a protein were normalized to the total spectral counts for that given data set. To account for multiple comparisons, the p values generated by the test were further adjusted using the Benjamini and Hochberg correction (26). An adjusted p value of 0.01 (*i.e.* 1% FDR) combined with a twofold change in expression was used to identify differentially expressed proteins in the reference proteomes comparison. An adjusted p value of 0.01 combined with a twofold increase in spectral count was used to identify adducted proteins.

Protein lists generated from different comparisons were visually compared using Venn diagrams generated by the Venny software package (27). To visualize the adduction pattern for adducted proteins, we used the "heatmap" function in R to generate heat maps. Spectral counts from biological replicates were averaged for the heat map visualization. Gene Gene Ontology (GO) and pathway enrichment analyses were performed using the WebGestalt software (28). (http://bioinfo.vanderbilt.edu/webgestalt). To compare the background protein abundance in three groups with different sensitivity to electrophile exposure, we used the Kruskal-Wallis test implemented in R (29). To visualize the network impact of protein alkylation by aHNE and aONE in both cell types, we used the Netgestalt tool (30).

Measurement of Cellular GSH—Cell pellets were resuspended in M-PER® Mammalian Protein Extraction Reagent (Thermo Scientific, Rockford, IL) and sonicated (10 pulses at 20% duty cycle). Lysates were cleared by centrifugation at 10000 rpm for 10 min and protein concentration was determined by the Bradford assay (Bio-Rad), according to the manufacturer's instructions. For GSH analysis in RKO cells, 100 μl of sample was mixed with 100 μl of 200 mM ammonium bicarbonate and 5 μl of 1000 pmol/μl internal standard solution (GSH ethyl ester)(Sigma, St Louis, MO). For GSH analysis in THP-1 cells, 100 μl of sample was mixed with 85 μl ammonium bicarbonate and 5 μl of 20 pmol/μl GSH ethyl ester internal standard solution. THP-1 samples were reduced with 25 μl of 200 mM dithiothreitol for 30 min at 60 °C. Samples were alkylated by adding 25 μl of 200 mM iodoethylacetate, and mixed by repeated inversion in the dark for 30 min at room temperature. Proteins were precipitated with 60 μl of cold sulfosalicylic acid solution (10% w/v) (31). The solution was centrifuged at 14,000 × g at 4 °C for 10 min, the supernatant (200 μl) was collected and stored at −20 °C until analysis.

Selected reaction monitoring analyses were performed on a Thermo TSQ Quantum Ultra triple-quadrupole MS instrument (ThermoFisher Scientific, San Jose, CA) equipped with an electrospray ionization source operated in positive mode and a Waters Acquity Sample Manager and Binary Solvent Manager. Samples were resolved on a 50 × 2.1 mm, 3 μm particle diameter Ascentis C18 column (Supelco, Bellefonte, PA) at a flow rate of 300 μl/min. Buffer A (0.1% formic acid in water) was held at 99% for 0.5 min then a linear gradient to 98% solvent B (0.1% formic acid in acetonitrile) was applied over the next 1.5 min. The column was washed at 2% A for 2 min and

equilibrated to 99% A for 3 min. The collision energy was set to 10eV for both analytes, and the *m/z* transitions measured were 394.2 -> 265.2 and 422.2 -> 293.2 for derivatized GSH and GSH ethyl ester, respectively.

Data were analyzed with Thermo Xcalibur software to measure area under the curve values for transitions corresponding to GSH and GSH ethyl ester. Absolute values for GSH were determined by normalizing GSH peak area to that for GSH ethyl ester; the calculated values were then normalized to the amount of protein present in each sample. Cellular GSH concentrations were determined by converting micrograms of protein to number of cells then to volume based on previously determined cell volumes for THP1 (32) and RKO (33) cells. Data were displayed graphically and statistical analyses were performed in GraphPad Prism using one-way ANOVA with a Tukey post test to $p < 0.05$.

Analysis of GSH-aHNE Metabolites—To measure the formation of GSH-aHNE conjugates, we incubated 80% confluent RKO and THP1 cells plated in 150 mm culture dishes with 100 μM aHNE or vehicle control delivered in serum-free culture media. Treatment was performed at 37 °C and stopped at different amounts of time between 0 and 2 h. Following treatment, medium (5 ml) and pelleted cell samples were flash frozen in liquid nitrogen to stop the reaction.

Cell treated pellets were resuspended in 500 μl of cold 50 mM HEPES buffer supplemented with 150 mM NaCl and 1 ml of cold methanol, sonicated (20 pulses, 20% duty cycle), and cleared by centrifugation at 10,000 $\times$ *g* for 10 min to remove cellular debris and the protein precipitate. The clear supernatant containing the metabolites as well as the treatment medium were further extracted with $CHCl_3$. To the medium (5 ml) were added 0.1 N HCl (2 ml) and $CHCl_3$ (5 ml); to the cell samples (1.5 ml) were added 0.1 N HCl (500 μl) and $CHCl_3$ (1 ml). All samples were vortex mixed, then centrifuged to separate the layers. The $CHCl_3$ layer was removed and reserved for the small molecule analysis described below. The internal standard, *N*-acetyltyrosine (0.10 μmol), was added to an aliquot (200 μl) of the aqueous phase and analyzed by LC/MS as further described in the results section.

Analysis of aHNE, aHNEA, and diol—The $CHCl_3$ layer from the previous step was concentrated and the sample was resuspended in H_2O:CH_3CN (400 μl, 3:1). 5-Hexyn-1-ol (1.0 μmol) was added as an internal standard. To improve ionization and detection by mass spectrometry, the samples were derivatized with 6-azidohexanoic acid to the triazole using Click chemistry. To each sample was added 6-azidohexanoic acid (2.5 μmol), TBTA ligand (2.5 μmol), sodium ascorbate (12.5 μmol), and $CuSO_4$ (12.5 μmol). The samples were allowed to react at room temperature for 1 h, than analyzed by LC/MS.

RESULTS

RKO and THP-1 Cells Express Similar Proteomes, but Different Susceptibilities to Alkylation Damage—We studied protein alkylation damage in the human colon adenocarcinoma cell line RKO and in human THP-1 macrophages, which we prepared by phorbol myristate acetate (PMA)-induced differentiation. aHNE and aONE display similar toxic potency (IC_{50} values ~20 μM (34)) in both cell models. To provide reference data for electrophile adduct studies, we first generated proteome inventories from untreated cells, which identified 3012 THP-1 proteins and 2820 RKO proteins (supplemental Tables S1 and S2). Of the 3233 proteins comprising the combined global inventories, 80% were found in both cell types. RKO cells showed higher expression of 607 proteins (Poisson FDR < 0.01, fold-change > 2), with Gene Ontology (GO) annotations characteristic of rapidly proliferating cells, including cell cycle and mitosis, carbon metabolism, protein and nucleic acid biosynthesis (supplemental Fig. S2 and supplemental Table S3). THP-1 cells showed higher expression of 778 proteins, with GO annotations characteristic of macrophage phenotypes, including cell-matrix adhesion, lipid metabolism, endocytosis, immune response and integrin-mediated signaling (supplemental Fig. S3 and supplemental Table S4).

RKO cells displayed a significantly greater ability to protect against alkylation damage by electrophile conjugation with reduced glutatione (GSH). Untreated RKO cells contained ~5 mM GSH (Fig. 1*A*), which is typical of many cell types. The differentiation of THP-1 monocytes to THP-1 macrophage cells with PMA reduced their GSH content dramatically, from ~1 mM to ~0.02 mM (Fig. 1*B*), as had been reported previously (35, 36). Although the THP-1 cells contained very low GSH levels, they did not display evidence of stress or lack of viability in the absence of electrophile treatment. Electrophile treatment of RKO cells produced a concentration-dependent depletion of GSH (Fig. 1*A*), whereas electrophiles produced little further depletion of GSH in THP-1cells (Fig. 1*C*).

When the two cell types were treated with aHNE, the rate of aHNE conjugation with GSH was almost 10-fold greater in RKO cells than in THP-1 cells (Fig. 1*D*). The enhanced ability of RKO cells to detoxify electrophiles is also consistent with the greater diversity and expression of glutathione-S-transferases in the RKO reference proteome (Table S2). Reactions of aHNE with medium proteins, GSH, amino acids and other nucleophilic medium constituents did not contribute significantly to aHNE consumption. Oxidative and reductive metabolism of aHNE to the corresponding carboxylic acid and diol, respectively, were detected, but did not differ between cell types. Thus, RKO and THP-1 cells provide models with similar proteomes, but with dramatically different capacity for GSH-dependent electrophile detoxication and different susceptibilities to protein alkylation.

Lipid Electrophiles Produce Widespread Protein Alkylation Damage—Treatment with aHNE and aONE produced widespread protein alkylation in both cell types. THP-1 cells were treated with 0, 5, 10, and 20 μM aHNE and aONE, whereas RKO cells were treated with 0, 10, 20, and 50 μM aHNE and aONE. We previously determined that the IC_{50} concentrations for HNE and ONE in both cell types were ~20 μM (34) and that HNE and ONE and their alkynyl analogs displayed identical toxicity concentration-response curves (16). These exposure ranges therefore span nontoxic and toxic concentrations in both cell types.

Adduct inventories for the electrophiles included proteins that were significantly adducted at any exposure concentration compared with untreated controls (supplemental Fig. S4). A total of 1634 proteins (53% of the reference proteome) were modified by either or both electrophiles in THP-1 cells (Fig. 2*A*). In RKO cells, 1119 proteins were targeted (40% of the

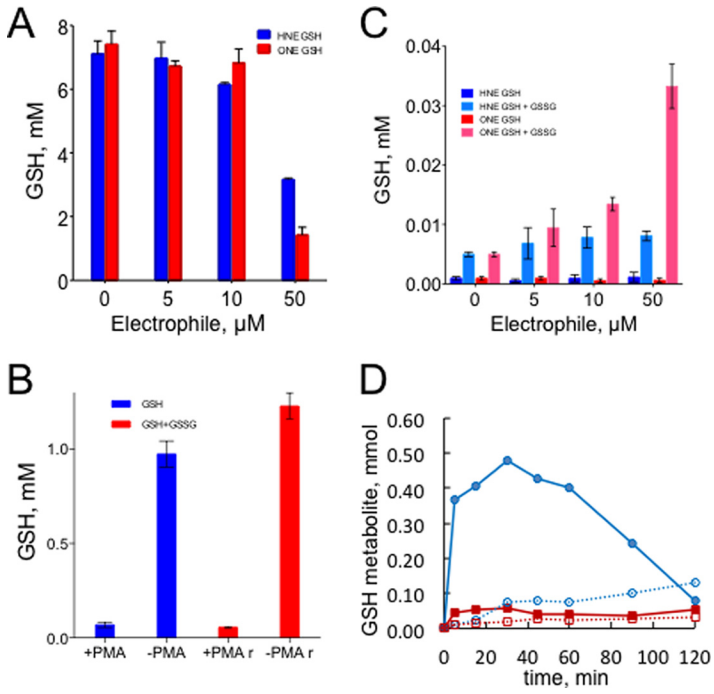

FIG. 1. **THP-1 and RKO cells have markedly different GSH content and THP-1 cells are deficient in GSH-dependent electrophile detoxication.** *A*, RKO cells contain millimolar levels of GSH, which is depleted by treatment with both aHNE and aONE. *B*, Differentiation of THP-1 monocytes to THP-1 macrophages with PMA reduces GSH content from ~1 mM to ~0.02 mM. Loss of GSH appears to result from loss of cellular glutatione equivalents, rather than formation of mixed disulfides, as reduction with 12.5 mM dithiothreitol (+PMAr and -PMAr) did not increase measured GSH. *C*, Treatment of THP-1 macrophages with aHNE and aONE did not further decrease GSH. *D*, RKO cells (circles), but not THP-1 cells (squares) efficiently detoxify aHNE by conjugation with GSH. aHNE-GS conjugates were measured in cells (filled symbols) and culture medium (open symbols) after treatment with 100 μM aHNE.

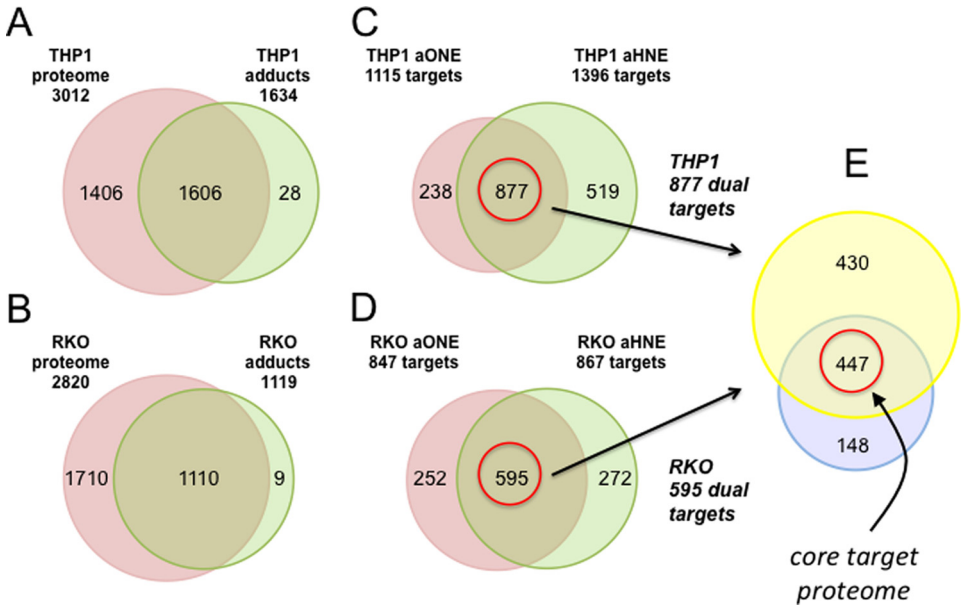

FIG. 2. **aHNE and aONE alkylated distinct sets of protein targets in THP-1 and RKO cell proteomes.** *A*, *B*, aHNE and aONE together alkylated approximately half of the THP-1 reference proteome and approximately half of the RKO reference proteome. *C*, *D*, aHNE and aONE targeted distinct sets of proteins in both THP-1 and RKO cells, together with substantial overlapping sets modified by both electrophiles and termed "dual targets." *E*, Overlap of the dual target proteomes identified a "core target proteome," consisting of protein targets of both electrophiles in both cell types.

reference proteome) (Fig. 2*B*). Approximately 50% of the proteins adducted in each cell line were targeted by both aHNE and aONE (Fig. 2*C* and 2*D*), whereas the remaining targets were distributed in approximately a 2:1 ratio between aHNE and aONE for THP1 cells, and in a 1:1 ratio between aHNE and aONE for RKO cells. (The full adduct inventories are presented in supplemental Tables S5 and S6).

Because aHNE and aONE exhibited similar IC_{50} concentrations in both cell lines, we initially hypothesized that proteins targeted by both electrophiles in both cell lines might be critical targets. Accordingly, we focused on those proteins that were adducted by both electrophiles in both the THP-1 and RKO inventories. Of the 1634 proteins adducted by aHNE or aONE in THP-1 cells, approximately half (877) were ad-

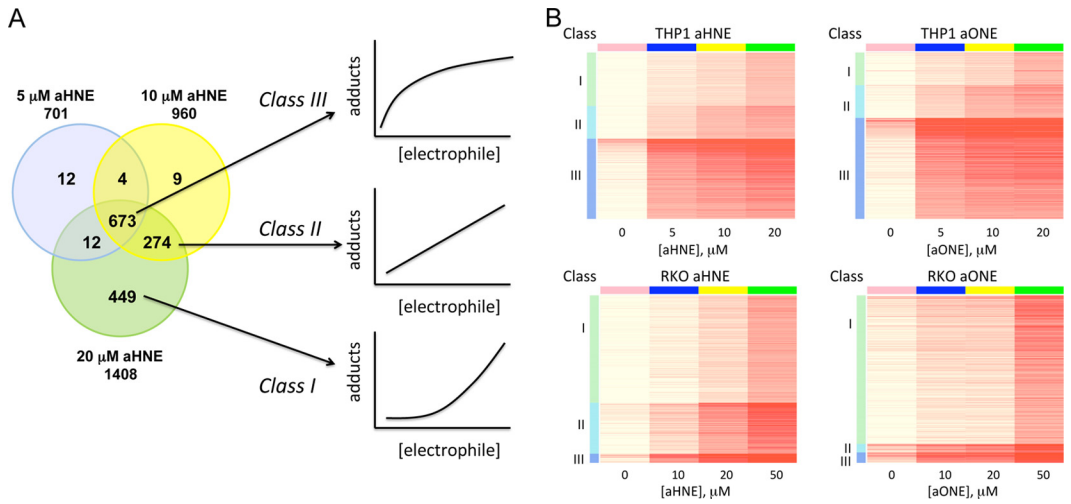

FIG. 3. **Concentration-dependent accumulation of protein adducts reveals three alkylation susceptibility classes.** *A*, Comparison of THP-1 cell proteins significantly alkylated at 5, 10 and 20 μM aHNE indicates three protein target classes. Class III proteins are significantly alkylated at all exposure concentrations, whereas Class II proteins are significantly alkylated only at 10 and 20 μM aHNE and Class I proteins are alkylated only at the 20 μM aHNE aHNE. The concentration-dependence of adduct accumulation for the three classes is illustrated in the accompanying representations. *B*, Heat maps illustrate dramatic differences in the distribution of electrophile target proteins between Classes I, II and III between THP-1 and RKO cells. The majority of aHNE and aONE targets in THP-1 cells are in Class III, which includes proteins with the highest susceptibility to alkylation. In contrast, most electrophile protein targets in RKO are in Class I, which has the lowest susceptibility to alkylation.

ducted by both electrophiles and we refer to these proteins as "dual targets" (Fig. 2*E* and supplemental Tables S7 and S8). In RKO cells, approximately half (595) of the 1119 adducted proteins were dual targets. Comparison of the two dual target lists identified 447 proteins that comprise a core target proteome—proteins adducted by both electrophiles in both cell types (Fig. 2*E* and supplemental Table S9).

Constituents of the core target proteome are significantly enriched in several GO biological process, molecular function and cellular compartment annotations mapping to gene expression and protein translation, DNA replication, protein folding and metabolism (supplemental Table S10 and supplemental Fig. S5), all of which could be plausibly linked to potential toxicity mechanisms. Nevertheless, mechanistic interpretation from this core target proteome is complicated by the fact that it represents proteome damage at both toxic and nontoxic exposure levels.

Approximately half of THP-1 and RKO proteins were not detectably adducted by either electrophile (supplemental Fig. S6*A*–S6*C*). (A complete listing of the nontarget proteins for THP-1 cells and RKO cells is provided in supplemental Tables S11 and S12, as well as proteins not adducted by either electrophile in both cell lines (supplemental Table S13)). We used WebGestalt (28) to identify protein GO biological process, molecular function and cellular compartment annotations significantly enriched for non-adducted proteins (supplemental Fig. S7 and supplemental Table S14). The most significant associations were for processes involved in electron transport and oxidative phosphorylation. These observations do not reflect limited access of aHNE and aONE to intramitochondrial proteins, as inspection of the protein target inventories (supplemental Tables S5 and S6) revealed adduction of numerous mitochondrial matrix proteins.

Concentration-dependence Identifies Different Protein Reactivity Classifications—We asked whether electrophile protein targets displayed distinct reactivity profiles, as had been observed in recent work (37). Examination of spectral count increases with increasing electrophile exposure concentration suggested that proteins differed significantly in susceptibility to adduction. Spectral count data for most of the adducted proteins did not fit a linear model, as we had described previously (13). Protein targets of aHNE and aONE can be grouped into three major classes reflecting the concentration-dependence of adduct accumulation (Fig. 3*A*). Class I target proteins were significantly adducted compared with unexposed controls only at the highest electrophile concentration (20 μM in THP-1 cells or 50 μM in RKO cells). Class II targets were significantly adducted at the medium and high concentrations (10 and 20 μM in THP-1 cells or 20 and 50 μM in RKO cells) and Class III targets were significantly adducted at all exposure concentrations. (Lists of all protein targets by classification in both cell types are provided in supplemental Tables S15 and S16.)

Protein target inventories expanded from Class III (most reactive) to Class I (least reactive) with increasing electrophile concentration, as shown in the heat maps in Fig. 3*B*. The heat maps illustrate the dramatic differences in protein alkylation susceptibility across the electrophile dose ranges for THP-1 cells *versus* RKO cells. In THP-1 cells, which display limited GSH-based detoxication, Class III targets comprised the larg-

est target category, whereas in the better-protected RKO cells, the fraction of Class III targets was small and Class I targets predominated. Of the Class III protein targets for aHNE and aONE in THP-1 cells, only 7% were Class III targets in RKO cells. Protein susceptibility to alkylation thus is highly dependent on cellular context, especially detoxification capacity.

Detection of adducted proteins in our analyses may be driven in part by abundance in the reference proteome. Given similar adduction stoichiometry, peptides from high-abundance proteins could be more easily detected by LC-MS/MS than those from low-abundance proteins. Indeed, for both aHNE and aONE targets, Class III targets were slightly, yet significantly more abundant than Class I and II targets in the corresponding reference proteomes for both THP-1 and RKO cells (Kruskall Wallis test $p < 2.2e-6$) (supplemental Fig. S8 and S9). Protein abundance thus contributes partially to the distribution of proteins among Classes I-III, most likely by affecting the detectability of proteins adducted at lower electrophile exposure concentrations.

Protein expression changes induced by electrophile treatment could affect detection of adducted proteins. Reduced protein expression may decrease detection of adducted protein, whereas increased protein expression could increase detection of adducted protein. To determine whether such expression changes were induced by electrophile treatment, we analyzed RKO cell proteins following a 6 h treatment with 0 or 45 μM aHNE. Poisson tests were performed between the treatment (45 μM aHNE) group and the control group (0 μM aHNE) identified only two significantly down-regulated proteins (FDR < 0.01, fold change < 0.5)—HRNR and KRT9. Of these two down-regulated proteins, KRT9 was found to be protected from adduction in RKO cells. The results of these comparisons are summarized in supplemental Table S17.

Electrophile Targets are Selectively Distributed across Functional Protein Interaction Networks—We used the Netgestalt tool (30) to vizualize the network impact of protein alkylation by aHNE and aONE in both cell types. Netgestalt places proteins in a protein-protein interaction network (38) in a linear order based on the hierarchical architecture of the network and displays the hierarchical network-module annotation below the ordered proteins. Therefore, it allows simultaneous overlay of the core target proteome and different protein adduct inventories over the protein-protein interaction network as parallel tracks (Fig. 4*A*) and enables easy zooming into network modules of interest (Fig. 4*B*). As noted above, aHNE and aONE adducted approximately half of the proteins in the THP-1 and RKO reference proteomes. However, inspection of the pattern of protein adduction in the core target proteome and individual cell types indicates selective damage across the protein interaction network. Specifically, constituents of the core target proteome are significantly enriched in ten network modules (Fisher's exact test, FDR<0.05) as indicated by colored asterisks in Fig. 4*A*. The majority of these modules are related to translation and mRNA processing (supplemental Table S18). Adduction patterns for individual cell lines and electrophiles are consistent with these statistical analyses. Moreover, display of tracks for protein adduct inventories as a function of electrophile concentration illustrates that increasing electrophile concentrations impact more protein network components, especially for the RKO cells. An expanded view (Fig. 4*B* and 4*C*) of the preferentially-targeted RNA splicing-related network module (highlighted by a blue asterisk in Fig. 4*A*) further illustrates the greater electrophile concentration-dependence for protein adduction in RKO cells than in THP-1 cells, which reflects differences in GSH-dependent detoxication. The same set of proteins in the RNA splicing module were targeted in the two cell lines, however, all of them belong to Class III in THP-1 cells, whereas all but one belong to Classes I and II in RKO cells. The impact of aHNE and aONE on RNA splicing proteins demonstrates a greater susceptibility of this subnetwork in THP-1 cells, despite similar expression of these proteins in both reference proteomes.

Because electrophiles selectively alkylated proteins in distinct protein interaction networks, we asked whether this pattern of damage could selectively impact functional biological processes. We used WebGestalt to evaluate GO biological process category enrichment of Class I, II, and III protein targets for each electrophile in both cell models (Fig. 5). (Full results of the enrichment analyses are presented in supplemental Tables S19–S22.) Electrophile protein targets in different reactivity classes were enriched for several GO biological processes. Class III aHNE targets in THP-1 cells were enriched for RNA metabolic processes and Class II and III aONE targets in both THP-1 and RKO cells were enriched for protein folding processes. Most strikingly in both cell models, Class II and III electrophile targets were enriched for processes involved in cytoskeletal regulation and Class I and II targets were enriched for processes involved in protein synthesis and turnover. GO biological processes involved in cytoskeletal regulation mapped to both actin- and tubulin-dependent processes whereas processes associated with protein synthesis and turnover included protein translation, translational elongation, the ubiquitin-proteasome system and other aspects of protein metabolism. Because Class III targets are significantly alkylated at the lowest electrophile concentrations, significant damage to cytoskeletal systems thereby occurs at non-toxic electrophile concentrations, whereas damage to systems associated with protein synthesis and turnover occurs at toxic electrophile concentrations.

DISCUSSION

This study describes the largest reported inventory of electrophile-mediated protein damage in intact cells and is the first to define the accumulation of damage as exposures progress from non-toxic to toxic electrophile concentrations. Our most important observation is that electrophiles target

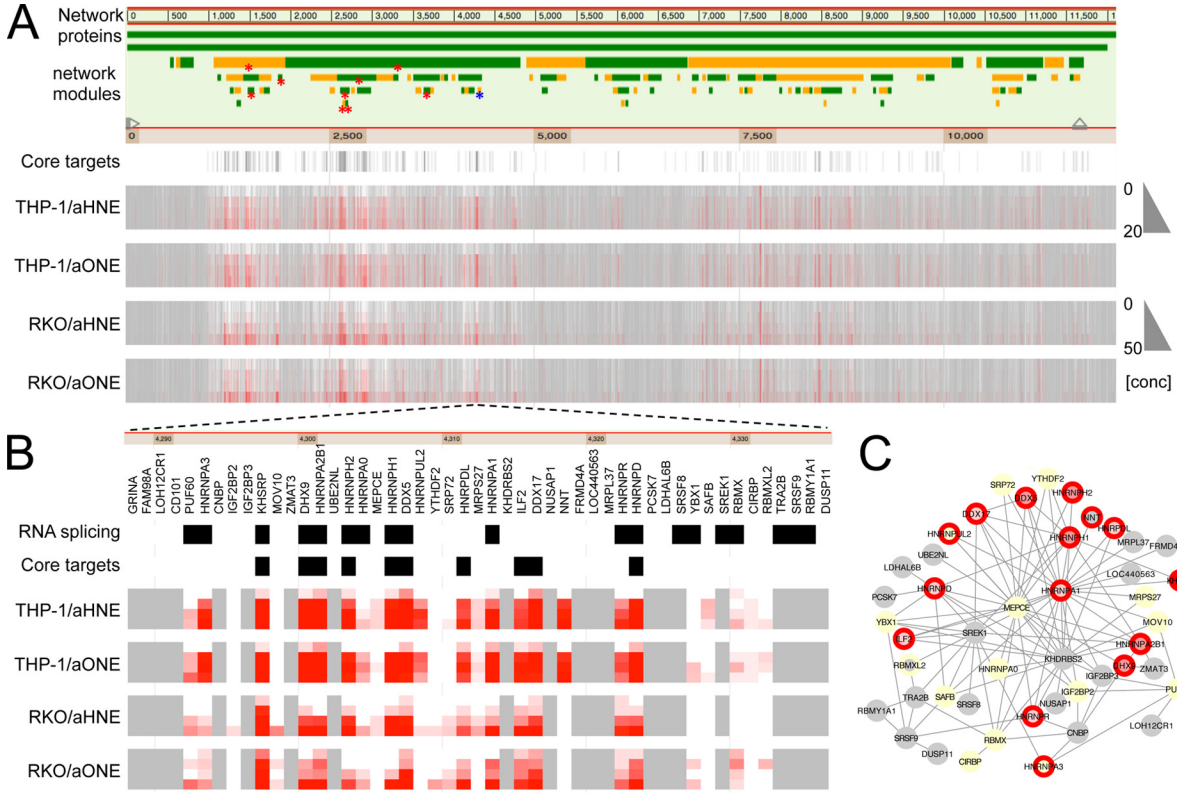

FIG. 4. **Electrophile alkylation occurs selectively across protein interaction networks.** *A*, Proteins in a protein-protein interaction network are placed in a linear order together with the hierarchical modular organization of the network. Alternating bar colors (green and orange) are used to distinguish neighboring modules. Preferentially adducted network modules are indicated by red and blue asterisks, and the latter is expanded in (*B*). The proteins in the core target proteome are visualized by black bars in the "Core targets" track. Network adduction data are visualized as heat maps with each row representing a concentration. Increasing darkness of red in the heat maps symbolizes increased level of adduction, whereas gray represents proteins not detected in the reference proteomes. Extensive alkylation in THP-1 cells at all concentrations contrasts with a clear concentration-dependent accumulation of adducts in RKO cells. *B*, Detailed view of a network module involved in RNA splicing. *C*, Link-node diagram of the RNA splicing module. Node color and node border color represent data for RKO/aHNE and THP-1/aHNE respectively, with the following color key: gray (not in reference proteomes), light yellow (nontarget), light red (Class I), medium red (Class II) and dark red (Class III).

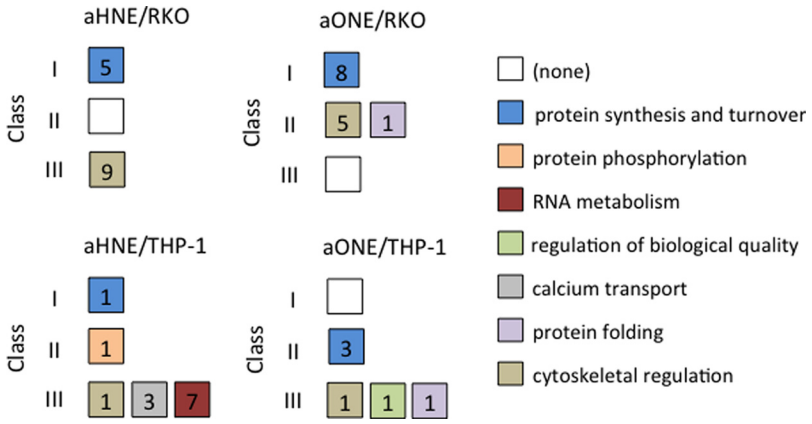

FIG. 5. **Electrophiles target distinct functional protein systems in protein alkylation susceptibility classes.** GO biological groups at right were based on shared proteins and functional similarity (GO biological processes significantly enriched for Class I, II, and III protein targets are listed in supplemental Tables S21 and S22). Numerals in the boxes indicating numbers of distinct GO biological processes within the groups are represented within each susceptibility class. Class II/III proteins were significantly enriched for GO biological processes involved in cytoskeletal regulation in both THP-1 and RKO cells. Class I/II proteins were significantly enriched for GO biological processes involved in protein synthesis and turnover in both THP-1 and RKO cells.

functional protein systems in a hierarchical manner. Proteins in the highest susceptibility class (Class III) were significantly enriched for GO biological processes associated with cytoskeletal function, whereas proteins in the lowest susceptibility class (Class I) were significantly associated with protein synthesis and turnover. Damage to Class I targets coincides with the onset of cell death, which suggests that damage to these protein systems constitutes lethal injury. Damage to Class III targets, such as cytoskeletal protein systems, occurs at nontoxic electrophile concentrations and may instead be survivable. The complete resistance of mitochondrial electron transport proteins to electrophile alkylation suggests that low reactivity toward electrophiles may preserve their essential functions. The data demonstrate that damage susceptibility differs between functional protein classes and suggest a hierarchy of critical protein functions for survival.

Previous work by us (10–13, 39) and others (9, 37, 40–42) identified cysteine residues as the principal targets of diverse electrophiles. Weerapana *et al.* used quantitative reactivity profiling of human cell lysates to identify a subset of 'hyperreactive' protein cysteine residues that were enriched for catalytic or other functional activities (37). We identified 50 electrophile protein targets that contain these hyperreactive cysteines (supplemental Table S23) and found that they were primarily Class III protein targets in THP-1 cells, which, like the lysates studied by Weerapana *et al.* had negligible GSH content. However, in RKO cells, most of these proteins were instead Class I or II targets, which indicates that GSH protection and possibly factors supersede intrinsic thiol reactivity as determinants of protein damage susceptibility.

GSH status dramatically affects profiles of covalent protein alkylation in both the RKO and THP-1 cell models. Nevertheless, the relationship between GSH status, protein adduction and toxicity suggests that GSH governs the former, but not the latter. In RKO cells, which have millimolar GSH, most protein targets are significantly alkylated only at the highest electrophile exposures (Class I), whereas in THP-1 cells, which have only micromolar GSH, most protein targets are significantly alkylated at all electrophile concentrations (Class III). This finding is consistent with the well-established view of GSH status as a critical cellular protectant against injury (15). Indeed, higher electrophile concentrations were required in the well-protected RKO cells to produce a comparable degree of protein adduction as in the nearly defenseless THP-1 cells.

These dramatic differences in susceptibility to covalent binding are surprising, given that the IC_{50} values for both HNE and ONE in both cell models are ~20 μM (34). Accumulation of a high overall level of protein damage thus does not account for the onset of lethal injury. In THP-1 cells at 20 μM aHNE and aONE, 1408 and 1124 proteins were adducted, whereas in RKO cells at the same electrophile concentrations, only 314 and 99 proteins were adducted, respectively and these totals increased only to 867 and 858 at 50 μM. Thus, the overall adduction load in the toxic concentration range for RKO cells was only about 25–50% of that in THP-1 cells. Moreover, cellular GSH measured at toxic electrophile treatment concentrations (50 μM) was ~2 mM, which is over 100-fold higher than in THP-1 cells (Fig. 1*B* and 1*C*). At toxic electrophile concentrations, the common feature of protein adduction in both cell lines is significant adduction of Class I proteins involved in protein synthesis and degradation processes. Thus, expansion of protein damage to critical systems, as opposed to overall protein alkylation levels, appeared to coincide with cell death.

A hierarchy of damage susceptibility may represent the evolution of functional protein systems to separate survivable from lethal injury and thereby allows cells to better withstand environmental stress. Mitochondrial electron transport systems are highly resistant to alkylation and are essential to life. Damage to protein synthesis, translation and turnover systems only occurs at toxic electrophile concentrations and the lower reactivity of these systems may protect these critical functions. Cytoskeletal proteins, protein folding, and metabolic quality control functions comprise the most susceptible systems and the ability of cells to withstand damage to these functions may be a key contributor to survival against constant, low-level environmental stress. Although little cell death occurs at the lowest electrophile treatment concentrations we studied, we have previously demonstrated activation of heat shock, ER stress, MAPK signaling, and other stress signaling responses at sublethal HNE concentrations in RKO cells (43–45). Thus, survivable damage to cytoskeletal systems may be accompanied by adaptive responses that contribute to cell survival.

Although our study focused on alkylation damage by analogs of endogenous lipid electrophiles associated with oxidative stress, an interesting question is whether a systems hierarchy for susceptibility to oxidative damage (*e.g.* thiol redox modifications) parallels that for alkylation damage. Weerapana *et al.* speculated that protein thiol nucleophilicity may have been evolutionarily selected to confer functional responsiveness to oxidative stress (37). This hypothesis could be tested with similar studies of thiol redox modifications, such as sulfenic acids (R-SOH), glutathionyl mixed disulfides (R-SSG) and nitrosothiols (R-SNO), all of which are amenable to targeted analysis by selective probes and Click chemistry-based analysis strategies (46, 47). Studies similar to those described here could determine whether a systems hierarchy governs the accumulation of thiol redox modifications in relevant models of oxidative damage.

Our data suggest new, testable hypotheses to resolve longstanding questions regarding drug toxicity. Although covalent protein alkylation is a feature of many hepatotoxic drugs, for example, the overall extent of binding does not adequately distinguish toxic from non-toxic binding (8, 48). Our data suggest that non-toxic covalent binding may largely be survivable damage to cytoskeletal components and other Class III protein targets, whereas toxic covalent binding produces

lethal injury by targeting protein synthesis and catabolism and possibly mitochondrial electron transport. Future studies with appropriate probe molecules for toxic and non-toxic drugs could test these hypotheses and provide a better mechanistic basis for interpreting protein alkylation in drug safety evaluation.

Acknowledgments—Raw data files, together with an IDPicker report (interactive document to view filtered peptide-to-spectrum matches and protein assembly information) and a README file are available at: *http://proteomics.ucsd.edu/ProteoSAFe/status.jsp?task=58c21b6e8fbc4922abf2cabf15ded4a0*. Click the ftp download link, then select the "Results" folder and follow the README instructions. The raw datafiles are contained in the "Spectrum" folder.

* This work was supported by National Institutes of Health Grants ES013125 and ES000267 and ES007028.

[S] This article contains supplemental Figs. S1 to S9 and Tables S1 to S23.

‖ To whom correspondence should be addressed: Department of Biochemistry, Vanderbilt University School of Medicine, U1213 MRBIII, 465 21st Ave. South, Nashville, TN 37232. Tel.: 615-322-3063; Fax: 615-343-8372; E-mail: daniel.liebler@vanderbilt.edu.

REFERENCES

1. Miller, E. C., Miller, J. A., Sapp, R. W., and Weber, G. M. (1949) Studies on the protein-bound aminoazo dyes formed in vivo from 4-dimethylaminoazobenzene and its C-monomethyl derivatives. *Cancer Res.* **9,** 336–343
2. Jollow, D. J., Mitchell, J. R., Potter, W. Z., Davis, D. C., Gillette, J. R., and Brodie, B. B. (1973) Acetaminophen-induced hepatic necrosis. II. Role of covalent binding in vivo. *J. Pharmacol. Exp. Ther.* **187,** 195–202
3. Evans, D. C., and Baillie, T. A. (2005) Minimizing the potential for metabolic activation as an integral part of drug design. *Curr. Opin. Drug Discov. Devel.* **8,** 44–50
4. Rudolph, T. K., and Freeman, B. A. (2009) Transduction of redox signaling by electrophile-protein reactions. *Sci. Signal.* **2,** re7
5. Schopfer, F. J., Cipollina, C., and Freeman, B. A. (2011) Formation and signaling actions of electrophilic lipids. *Chem. Rev.* **111,** 5997–6021
6. West, J. D., and Marnett, L. J. (2006) Endogenous reactive intermediates as modulators of cell signaling and cell death. *Chem. Res. Toxicol.* **19,** 173–194
7. Streeter, A. J., Bjorge, S. M., Axworthy, D. B., Nelson, S. D., and Baillie, T. A. (1984) The microsomal metabolism and site of covalent binding to protein of 3′-hydroxyacetanilide, a nonhepatotoxic positional isomer of acetaminophen. *Drug Metab. Dispos.* **12,** 565–576
8. Bauman, J. N., Kelly, J. M., Tripathy, S., Zhao, S. X., Lam, W. W., Kalgutkar, A. S., and Obach, R. S. (2009) Can in vitro metabolism-dependent covalent binding data distinguish hepatotoxic from nonhepatotoxic drugs? An analysis using human hepatocytes and liver S-9 fraction. *Chem. Res. Toxicol.* **22,** 332–340
9. Weerapana, E., Simon, G. M., and Cravatt, B. F. (2008) Disparate proteome reactivity profiles of carbon electrophiles. *Nat. Chem. Biol.* **4,** 405–407
10. Dennehy, M. K., Richards, K. A., Wernke, G. R., Shyr, Y., and Liebler, D. C. (2006) Cytosolic and nuclear protein targets of thiol-reactive electrophiles. *Chem. Res. Toxicol.* **19,** 20–29
11. Shin, N. Y., Liu, Q., Stamer, S. L., and Liebler, D. C. (2007) Protein targets of reactive electrophiles in human liver microsomes. *Chem. Res. Toxicol.* **20,** 859–867
12. Wong, H. L., and Liebler, D. C. (2008) Mitochondrial protein targets of thiol-reactive electrophiles. *Chem. Res. Toxicol.* **21,** 796–804
13. Codreanu, S. G., Zhang, B., Sobecki, S. M., Billheimer, D. D., and Liebler, D. C. (2009) Global analysis of protein damage by the lipid electrophile 4-hydroxy-2-nonenal. *Mol. Cell. Proteomics* **8,** 670–680
14. Zhang, B., Shi, Z., Duncan, D. T., Prodduturi, N., Marnett, L. J., and Liebler, D. C. (2011) Relating protein adduction to gene expression changes: a systems approach. *Mol. Biosyst.* **7,** 2118–2127
15. DeLeve, L. D., and Kaplowitz, N. (1991) Glutathione metabolism and its role in hepatotoxicity. *Pharmacol. Ther.* **52,** 287–305
16. Vila, A., Tallman, K. A., Jacobs, A. T., Liebler, D. C., Porter, N. A., and Marnett, L. J. (2008) Identification of protein targets of 4-hydroxynonenal using click chemistry for ex vivo biotinylation of azido and alkynyl derivatives. *Chem. Res. Toxicol.* **21,** 432–444
17. Kim, H. Y., Tallman, K. A., Liebler, D. C., and Porter, N. A. (2009) An azido-biotin reagent for use in the isolation of protein adducts of lipid-derived electrophiles by streptavidin catch and photorelease. *Mol. Cell. Proteomics* **8,** 2080–2089
18. Ham, A. J., Caprioli, R. M., and Gross, M. L. (2005) Proteolytic Digestion Protocols. *The Encyclopedia of Mass Spectrometry, Volume 2 Biological Applications Part A: Peptides and Proteins*, pp. 10–17, Elsevier Ltd., Kidlington, Oxford, UK
19. Ma, Z. Q., Tabb, D. L., Burden, J., Chambers, M. C., Cox, M. B., Cantrell, M. J., Ham, A. J., Litton, M. D., Oreto, M. R., Schultz, W. C., Sobecki, S. M., Tsui, T. Y., Wernke, G. R., and Liebler, D. C. (2011) Supporting tool suite for production proteomics. *Bioinformatics* **27,** 3214–3215
20. Tabb, D. L., Fernando, C. G., and Chambers, M. C. (2007) MyriMatch: highly accurate tandem mass spectral peptide identification by multivariate hypergeometric analysis. *J. Proteome Res.* **6,** 654–661
21. Zhang, B., Chambers, M. C., and Tabb, D. L. (2007) Proteomic parsimony through bipartite graph analysis improves accuracy and transparency. *J. Proteome Res.* **6,** 3549–3557
22. Ma, Z. Q., Dasari, S., Chambers, M. C., Litton, M. D., Sobecki, S. M., Zimmerman, L. J., Halvey, P. J., Schilling, B., Drake, P. M., Gibson, B. W., and Tabb, D. L. (2009) IDPicker 2.0: Improved protein assembly with high discrimination peptide identification filtering. *J. Proteome Res.* **8,** 3872–3881
23. Elias, J. E., and Gygi, S. P. (2007) Target-decoy search strategy for increased confidence in large-scale protein identifications by mass spectrometry. *Nat. Methods* **4,** 207–214
24. Thompson, D. K., Chourey, K., Wickham, G. S., Thieman, S. B., VerBerkmoes, N. C., Zhang, B., McCarthy, A. T., Rudisill, M. A., Shah, M., and Hettich, R. L. (2010) Proteomics reveals a core molecular response of Pseudomonas putida F1 to acute chromate challenge. *BMC Genomics* **11,** 311
25. Chourey, K., Thompson, M. R., Shah, M., Zhang, B., Verberkmoes, N. C., Thompson, D. K., and Hettich, R. L. (2009) Comparative temporal proteomics of a response regulator (SO2426)-deficient strain and wild-type Shewanella oneidensis MR-1 during chromate transformation. *J. Proteome Res.* **8,** 59–71
26. Benjamini, Y., and Hochberg, Y. (1995) Controlling the False Discovery Rate - a Practical and Powerful Approach to Multiple Testing. *J. Royal Statist. Soc.* **57,** 289–300
27. Ontiveros, J. C. (2007) VENNY. An interactive tool for comparing lists with Venn Diagrams. http://bioinfogp.cnb.csic.es/tools/venny/index.html
28. Zhang, B., Kirov, S., and Snoddy, J. (2005) WebGestalt: an integrated system for exploring gene sets in various biological contexts. *Nucleic Acids Res.* **33,** W741–W748
29. Hollander, M., Wolfe, D.A. (1973) *Nonparametric Statistical Methods*, John Wiley & Sons, New York
30. Shi, Z., Wang, J., and Zhang, B. (2013) NetGestalt: integrating multidimensional omics data over biological networks. *Nat. Methods* **10,** 597–598
31. Bouligand, J., Deroussent, A., Paci, A., Morizet, J., and Vassal, G. (2006) Liquid chromatography-tandem mass spectrometry assay of reduced and oxidized glutathione and main precursors in mice liver. *J. Chromatogr.* **832,** 67–74
32. Gallin, E. K., Mason, T. M., and Moran, A. (1994) Characterization of regulatory volume decrease in the THP-1 and HL-60 human myelocytic cell lines. *J. Cell. Physiol.* **159,** 573–581
33. Hope, C., Planutis, K., Planutiene, M., Moyer, M. P., Johal, K. S., Woo, J., Santoso, C., Hanson, J. A., and Holcombe, R. F. (2008) Low concentrations of resveratrol inhibit Wnt signal throughput in colon-derived cells: implications for colon cancer prevention. *Mol. Nutr. Food Res. 52 Suppl* **1,** S52–S61
34. McGrath, C. E., Tallman, K. A., Porter, N. A., and Marnett, L. J. (2011) Structure-activity analysis of diffusible lipid electrophiles associated with phospholipid peroxidation: 4-hydroxynonenal and 4-oxononenal analogues. *Chem. Res. Toxicol.* **24,** 357–370
35. El Fadili, K., Messier, N., Leprohon, P., Roy, G., Guimond, C., Trudel, N., Saravia, N. G., Papadopoulou, B., Legare, D., and Ouellette, M. (2005) Role of the ABC transporter MRPA (PGPA) in antimony resistance in

Leishmania infantum axenic and intracellular amastigotes. *Antimicrob. Agents Chemother.* **49,** 1988–1993
36. Seo, G. S., Lee, S. H., Choi, S. C., Choi, E. Y., Oh, H. M., Choi, E. J., Park, D. S., Kim, S. W., Kim, T. H., Nah, Y. H., Kim, S., Kim, S. H., You, S. H., and Jun, C. D. (2006) Iron chelator induces THP-1 cell differentiation potentially by modulating intracellular glutathione levels. *Free Radic. Biol. Med.* **40,** 1502–1512
37. Weerapana, E., Wang, C., Simon, G. M., Richter, F., Khare, S., Dillon, M. B., Bachovchin, D. A., Mowen, K., Baker, D., and Cravatt, B. F. (2010) Quantitative reactivity profiling predicts functional cysteines in proteomes. *Nature* **468,** 790–795
38. Turinsky, A. L., Razick, S., Turner, B., Donaldson, I. M., and Wodak, S. J. (2011) Interaction databases on the same page. *Nat. Biotechnol.* **29,** 391–393
39. Connor, R. E., Marnett, L. J., and Liebler, D. C. (2011) Protein-selective capture to analyze electrophile adduction of hsp90 by 4-hydroxynonenal. *Chem. Res. Toxicol.* **24,** 1275–1282
40. Carbone, D. L., Doorn, J. A., Kiebler, Z., Ickes, B. R., and Petersen, D. R. (2005) Modification of heat shock protein 90 by 4-hydroxynonenal in a rat model of chronic alcoholic liver disease. *J. Pharmacol. Exp. Ther.* **315,** 8–15
41. Chavez, J., Chung, W. G., Miranda, C. L., Singhal, M., Stevens, J. F., and Maier, C. S. (2010) Site-specific protein adducts of 4-hydroxy-2(E)-nonenal in human THP-1 monocytic cells: protein carbonylation is diminished by ascorbic acid. *Chem. Res. Toxicol.* **23,** 37–47
42. Groeger, A. L., Cipollina, C., Cole, M. P., Woodcock, S. R., Bonacci, G., Rudolph, T. K., Rudolph, V., Freeman, B. A., and Schopfer, F. J. (2010) Cyclooxygenase-2 generates anti-inflammatory mediators from omega-3 fatty acids. *Nat. Chem. Biol.* **6,** 433–441
43. West, J. D., and Marnett, L. J. (2005) Alterations in gene expression induced by the lipid peroxidation product, 4-hydroxy-2-nonenal. *Chem. Res. Toxicol.* **18,** 1642–1653
44. Jacobs, A. T., and Marnett, L. J. (2007) Heat shock factor 1 attenuates 4-Hydroxynonenal-mediated apoptosis: critical role for heat shock protein 70 induction and stabilization of Bcl-XL. *J. Biol. Chem.* **282,** 33412–33420
45. Jacobs, A. T., and Marnett, L. J. (2009) HSF1-mediated BAG3 expression attenuates apoptosis in 4-hydroxynonenal-treated colon cancer cells via stabilization of anti-apoptotic Bcl-2 proteins. *J. Biol. Chem.* **284,** 9176–9183
46. Paulsen, C. E., and Carroll, K. S. (2013) Cysteine-Mediated Redox Signaling: Chemistry, Biology, and Tools for Discovery. *Chem Rev.* **113,** 4633–4679
47. Doulias, P. T., Tenopoulou, M., Raju, K., Spruce, L. A., Seeholzer, S. H., and Ischiropoulos, H. (2013) Site specific identification of endogenous S-nitrosocysteine proteomes. *J Proteomics.* **92,** 195–203
48. Bauman, J. N., Frederick, K. S., Sawant, A., Walsky, R. L., Cox, L. M., Obach, R. S., and Kalgutkar, A. S. (2008) Comparison of the bioactivation potential of the antidepressant and hepatotoxin nefazodone with aripiprazole, a structural analog and marketed drug. *Drug Metab. Dispos.* **36,** 1016–1029